

Heisenberg limited single-mode quantum metrology

W. Wang,^{1,*} Y. Wu,^{1,2,*} Y. Ma,¹ W. Cai,¹ L. Hu,¹ X. Mu,¹ Y. Xu,¹ Zi-Jie Chen,³ H. Wang,¹ Y. P. Song,¹ H. Yuan,⁴ C.-L. Zou,³ L.-M. Duan,¹ and L. Sun¹

¹Center for Quantum Information, Institute for Interdisciplinary Information Sciences, Tsinghua University, Beijing 100084, China

²Department of Physics, University of Michigan, Ann Arbor, Michigan 48109, USA

³Key Laboratory of Quantum Information, CAS, University of Science and Technology of China, Hefei, Anhui 230026, P. R. China

⁴Chinese University of Hong Kong, Hong Kong, China

Two-mode interferometers, such as Michelson interferometer based on two spatial optical modes, lay the foundations for quantum metrology [1–3]. Instead of exploring quantum entanglement in the two-mode interferometers, a single bosonic mode also promises a measurement precision beyond the shot-noise limit (SNL) by taking advantage of the infinite-dimensional Hilbert space of Fock states [4]. However, the experimental demonstration still remains elusive. Here, we demonstrate a single-mode phase estimation that approaches the Heisenberg limit (HL) unconditionally. Due to the strong dispersive nonlinearity and long coherence time of a microwave cavity, quantum states of the form $(|0\rangle + |N\rangle)/\sqrt{2}$ are generated, manipulated and detected with high fidelities, leading to an experimental phase estimation precision scaling as $\sim N^{-0.94}$. A 9.1 dB enhancement of the precision over the SNL at $N = 12$, which is only 1.7 dB away from the HL, is achieved. Our experimental architecture is hardware efficient and can be combined with the quantum error correction techniques to fight against decoherence [5, 6], thus promises the quantum enhanced sensing in practical applications.

Based on the coherent interference effects, interferometers have been extensively used in precision measurements. For example, the two-mode atomic Ramsey interferometer that manipulates the superpositions of two internal states of an atomic ensemble has been used in various applications, such as clock, gravimeter, and gyro [7]. Similarly, by separating photons into two spatial modes, two-mode photonic Michelson interferometers have been extensively used in LIGO [8], optical coherence tomography and spectrometer. Recently, quantum metrology, which makes use of quantum mechanical effects, such as entanglement, has gained a lot of attention in the two-mode interferometers, as it can achieve measurement precisions beyond the classical limit [1–3, 9, 10]. In the applications of quantum metrology, highly entangled states, such as the Greenberger–Horne–Zeilinger state of an atomic ensemble [2, 3] or the NOON state of optical interferometer [11, 12], are essential. To prepare these exotic quantum states, non-local operations are required. In addition, the optimal measurements are also typically highly non-local. This poses significant challenges for practical applications of quantum metrology.

In this Letter, instead of exploring quantum entanglement in the two-mode interferometer we implement the single-mode photonic quantum metrology with a superconducting qubit-oscillator system [13] and demonstrate an unconditional phase estimation with the precision approaching the HL. A quantum sensor with a single mode is of great interest [4, 14] for its hardware efficiency, compactness, and robustness against non-local perturbations. For a single mode, the phase can be measured based on the photon number dependent phase accumulation. Using the state $|\Psi(N)\rangle = (|0\rangle + |N\rangle)/\sqrt{2}$, superpositions of Fock states, up to $N = 12$, we demonstrate a phase estimation precision which scales as $\delta\tilde{\theta} \sim N^{-0.94}$ and approaches the HL. At $N = 12$, $\delta\tilde{\theta}$ corresponds to an enhancement of $20\log_{10}(\delta\tilde{\theta}_{\text{SNL}}/\delta\tilde{\theta})$ dB = 9.1 dB over the SNL $\delta\tilde{\theta}_{\text{SNL}}$. Envisioning future applications in the optical

regime with microwave-to-optical transduction, we also realize a measurement scheme that is easy to implement in optics and only uses displacement operations and photon counting. Under this restricted measurement scheme, an SNL-beating precision, which scales as $\delta\tilde{\theta} \sim N^{-0.62}$, is also achieved.

According to the quantum Cramer-Rao bound [15], the estimation precision of parameter θ encoded in the state $|\psi(\theta)\rangle = e^{-i\theta H}|\psi\rangle$ is lower bounded as $\delta\tilde{\theta} \geq \frac{1}{2\Delta H}$, where $\delta\tilde{\theta}$ is the standard deviation of an unbiased estimator $\tilde{\theta}$, and $(\Delta H)^2 = \langle\psi|H^2|\psi\rangle - \langle\psi|H|\psi\rangle^2$ is the variance of the Hamiltonian H under the initial probe $|\psi\rangle$. The quantum states with a maximum variance therefore are optimal for the single-mode sensing, i.e. the equal superpositions of the eigenstates of H corresponding to the extreme eigenvalues are the most preferable quantum states. For example, as illustrated in Figs. 1a and 1b, an atom prepared in the equal superposition of angular momentum states $|J, -J\rangle$ and $|J, J\rangle$ has maximal sensitivity to external field ($H = J_z$ and J_z is the angular momentum operator). Recently, a high precision electrometer, using the Schrödinger cat state of large angular momentum states to enhance ΔH , has also been demonstrated to beat SNL [16–18]. Similarly, the phase precision with a single bosonic mode would be enhanced by using the state $|\Psi(N)\rangle = (|0\rangle + |N\rangle)/\sqrt{2}$, since it has the maximum variance for $H = a^\dagger a$ (a is the bosonic operator of the sensing mode) (Figs. 1c and 1d). Such a maximum variance state (MVS) can in principle achieve the HL precision $\delta\tilde{\theta} = 1/N$ with \sqrt{N} times enhancement over the SNL.

As schematically illustrated in Figs. 1e and 1f, our experiment is carried out with a superconducting system consisting of a transmon qubit dispersively coupled to two three-dimensional cavities [5, 6, 19]. One long-lived cavity serves as the sensing mode; the transmon qubit as an ancilla assists the preparation, manipulation and detection of the photonic states in the sensing mode; the short-lived cavity is employed for a high-fidelity readout of the qubit state. The Hamiltonian of the qubit-oscillator system is $H = -\hbar\chi_{\text{qs}}a^\dagger a|e\rangle\langle e|$ [13],

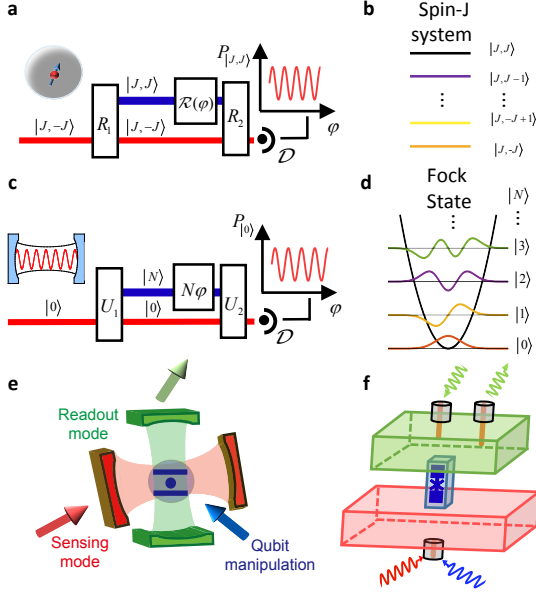


FIG. 1: **Single-mode quantum metrology architectures.** **a** and **b** Single-atom Ramsey interferometer with a total angular momentum number J . The best precision can be achieved by using the superposition of $|J, -J\rangle$ and $|J, J\rangle$ with the maximum variance of angular momentum. **c** and **d** Single-mode Ramsey interferometer for photons/bosons with an optimal precision achieved by the superposition of Fock states with the maximal variance of photon numbers for a given mean photon number. **e** and **f** Schematic illustrations of the single-mode sensing architecture and the experimental circuit quantum electrodynamics system. A single qubit couples to two photonic cavity modes, with the two modes serving as the sensing mode and the ancillary qubit readout mode, respectively. The two boxes represent the microwave cavities, between which the ancillary superconducting qubit on a chip is located in a waveguide trench.

where $|e\rangle$ is the excited state of the qubit (the ground state is $|g\rangle$), and χ_{qs} reflects the dispersive interaction strength between the qubit and the mode. In our system, $\chi_{qs}/2\pi = 1.90\text{MHz}$ is much stronger than the decoherence rates of the qubit and the sensing mode, thus allows full control of the photonic quantum state [5, 6, 20–22].

In our experiment, the probe states of the sensing mode are deterministically created by implementing a qubit-assisted unitary operation on the mode. With numerically optimized control pulses [23], the probe states $|\Psi(N)\rangle = (|0\rangle + |N\rangle)/\sqrt{2}$ with $N = 1, 2, \dots, 12$ are prepared faithfully. In Fig. 2 the experimentally measured Wigner functions (bottom panels) of the typical MVSs are plotted, agreeing well with the ideal ones (top panels). In the phase-space, there are interesting periodic fringes in the polar direction with N -fold rotational symmetry for $|\Psi(N)\rangle$. As the rotation of the Wigner function by θ corresponds to the phase operation $U(\theta) = e^{i\theta a^\dagger a}$ on the oscillator, the enhanced measurement precision by the MVS can be intuitively explained: because of the fine fringe features, $|\Psi(N)\rangle$ would be rotated to an orthogonal state when the phase $\theta = \pi/N$, the measurement precision with the MVS is thus proportional to N , instead of \sqrt{N} .

Figure 3a depicts the experimental circuit for the optimal sensing scheme by a Ramsey-like interference (Fig. 1c), which is potential for attaining the ultimate precision HL for the single-mode sensing. After an initialization process, the cavity is prepared in $|\Psi(N)\rangle$ while the qubit ends up with $|e\rangle$, resulting in a phase operation $U(\theta)$ on the sensing mode with $\theta = -\chi_{qs}\tau$ and τ being the waiting time. Then, a unitary U_H is implemented to rotate $|\Phi_+\rangle = |e\rangle(|0\rangle + |N\rangle)/\sqrt{2}$ to $|g\rangle|0\rangle$ and $|\Phi_-\rangle = |e\rangle(|0\rangle - |N\rangle)/\sqrt{2}$ to $|e\rangle|0\rangle$. Finally, the ancillary qubit is projectively measured on $|g\rangle$, giving projection of $U(\theta)|\Psi(N)\rangle$ onto $|\Psi(N)\rangle$ with the ideal probability oscillation $P_{\text{opt}}^{(N)} = (1 + \cos N\theta)/2$.

The experimental results of the optimal scheme $P_{\text{opt}}^{(N)}$ are shown in Fig. 3b. As intuitively expected from Fig. 2, the period of the Ramsey interference fringes reduces with N and the contrast of the fringes are nearly ideal. By fitting the experimentally measured probability with $P^{(N)}(\theta) = A + B\cos(N\theta)$, where $A - B$ and B represent the detected background and the contrast of the Ramsey interference fringes, respectively, the phase estimation precision can be inferred as $\delta\tilde{\theta} = \sqrt{P^{(N)}(\theta)(1 - P^{(N)}(\theta))} / \frac{\partial P^{(N)}(\theta)}{\partial \theta} = \frac{\sqrt{A(1-A)}}{NB}$.

Figure 3c shows the results of $\delta\tilde{\theta}$ (blue dots) as a function of N in a logarithmic-logarithmic scale. Clearly, the optimal scheme beats the SNL, with the green region representing the experimental results that surpass the SNL with a maximum precision enhancement of 9.1 dB at $N = 12$, which is only 1.7 dB away from the ultimate HL. The results demonstrate the quantum advantage of our single-mode sensing unambiguously. The obtained precision scales as $N^{-0.94}$, approaching the Heisenberg scaling (N^{-1}). The slight deviation mainly attributes to the N -dependent imperfections including the larger operation errors for larger Hilbert space of Fock states (errors in the control pulse and parameter uncertainties) and higher probability of photon loss.

The demonstrated optimal schemes can be utilized in practical sensing applications, for example, the detection of the frequency and power of a microwave signal based on the Stark-effect-induced phase shift of the sensing mode. By utilizing the recently developed high-efficient bidirectional microwave-to-optical quantum transduction [24, 25], our scheme with the MVS can also be employed for the optical metrology. However, the Ramsey-like measurement is very challenging in optical domain due to the limited capability of deterministic quantum state manipulation of optical photons. We thus propose a hybrid sensing scheme, as shown in Fig. 4a, by employing a measurement scheme that only uses easy operations in the optical domain, such as displacement operation and photon counting [26].

Envisioning the application of such a hybrid scheme, we simulate the scheme in our superconducting system with the restricted measurement. It is worth noting that different from photon counting in the real optical system [26], the measurement through the ancillary qubit in the superconducting system can only obtain a binary output, i.e. a

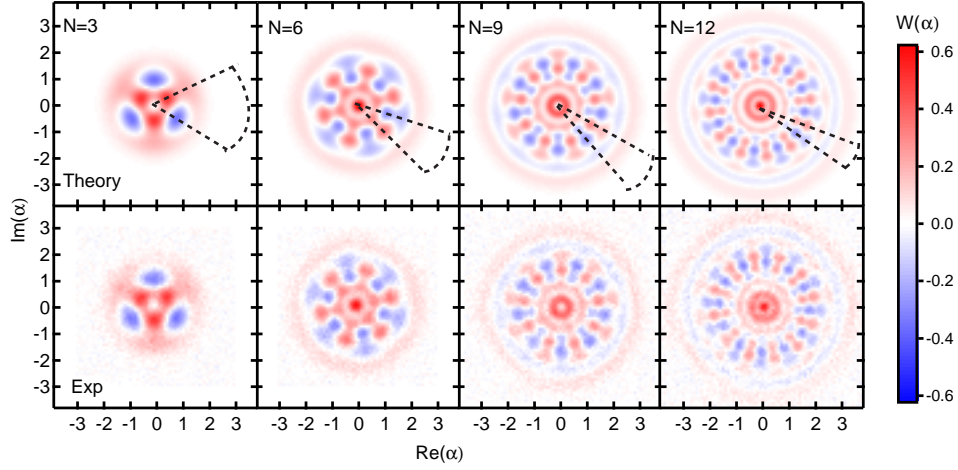


FIG. 2: **Wigner functions of the maximum variance states.** Theoretical (top panel) and experimental (bottom panel) results for $N = 3, 6, 9, 12$ with state fidelities of 0.94, 0.92, 0.83, 0.70, respectively. The measured state preparation fidelity decays with N , mainly attributed to the larger probability of photon loss and the worse reconstruction measurement to obtain the Wigner functions for larger N . The measured range of the real and imaginary parts of α is $[-3.0, 2.9]$ for $N = 3$ and 6, $[-3.6, 3.5]$ for $N = 9$, and $[-3.9, 3.8]$ for $N = 12$. The angles of the dashed sectors indicate that the sensitivity of phase estimation scales as $1/N$.

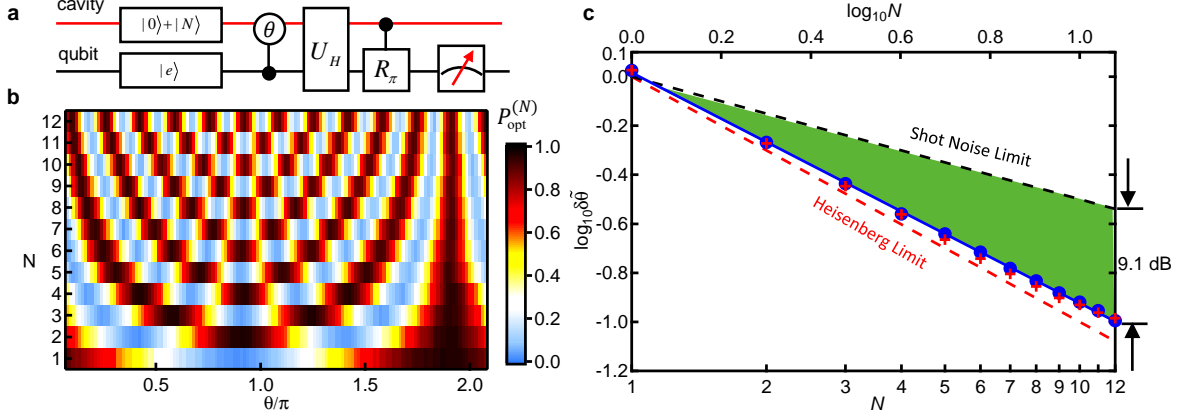


FIG. 3: **Optimal single-mode sensing scheme.** **a** Quantum circuit. **b** The measured probability $P_{\text{opt}}^{(N)}$ of projecting to $|\Psi(N)\rangle$ as a function of the phase θ in the optimal scheme for different N . The outcomes are obtained with 10^6 repetitions of the experiment. **c** Quantum advantage of the optimal scheme. Blue dots are experimental results. The blue solid line is a linear fit and gives $\log_{10} \delta\theta = -0.94 \log_{10} N + 0.016$ with the precision scaling $N^{-0.94}$ approaching the Heisenberg scaling (N^{-1}). The small offset 0.016 in the log-log scale of the precision is dominantly due to the imperfections of the qubit readout process, where the spontaneous decay of the qubit gives wrong indication of the cavity state and lowers the contrast of the Ramsey interference. The red crosses are the results from numerical simulations including the decoherences of our system, in good agreement with the measured data. The black and red dashed lines are the theoretically calculated SNL and HL, respectively. Green region represents the experimental results that surpass the standard limit by about 9.1 dB at $N = 12$. Error bars are smaller than the markers.

result of whether the photon number is n or not. So, the outcome of the measurement has the probability $P_n^{(N)} = |\langle n|D(\alpha)U(\varphi)|\Psi(N)\rangle|^2$, where $D(\alpha)$ is the displacement operator and $U(\varphi) = \exp(-i\varphi a^\dagger a)$ is the phase operator. We optimize the parameters α and n for each MVS to maximize the measurement precision (see Supplementary Materials).

The experimental results for the simulated hybrid scheme are summarized in Fig. 4b. Although the fringe period reduces with N similar to that in the optimal scheme, the contrast for the hybrid scheme reduces with N . The reason is mainly that the probability of the binary photon number detection reduces

for large N as the state spreads in the Fock space after a displacement operation. However, this hybrid scheme beats the SNL as well, as indicated by the green region in Fig. 4c, with a maximum precision enhancement of 0.7 dB at $N = 12$. The obtained scaling $N^{-0.62}$ ($N^{-0.69}$ for an ideal experiment) is lower than that for the optimal scheme because of the sub-optimal detection process, but can still beat the standard scaling $N^{-0.5}$ due to the initial MVS. Actually, by using a photon number resolving detector, which is available in optical domain, a better precision could be achieved by the hybrid scheme in future optical sensing applications (as shown by

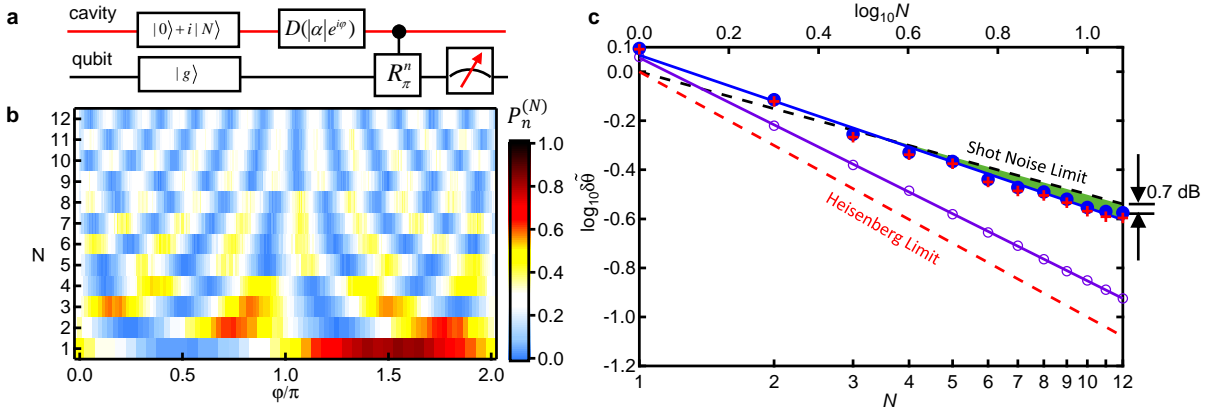


FIG. 4: **Hybrid single-mode sensing scheme.** **a** Quantum circuit. The phase operation $U(\varphi) = \exp(-i\varphi a^\dagger a)$ is effectively added to the sensing mode in the rotating-frame of the displacement operation. The detection is realized by a combination of a displacement of the photonic mode $[D(\alpha = |\alpha|e^{i\varphi})]$ and selective photon number ($|n\rangle$ state) detection enabled by the ancillary qubit through its dispersive interaction to photons. **b** The measured probability $P_n^{(N)}$ of projecting to the photon number state $|n\rangle$ as a function of φ in the displacement operation, with the optimal n_{opt} for each N being numerically obtained. **c** Quantum advantage for the hybrid scheme. Blue dots are experimental results. The blue solid line is a linear fit and gives $\log_{10} \delta\theta = -0.62 \log_{10} N + 0.068$. The red crosses are the results from numerical simulations including the decoherences of our system, in good agreement with the measured data. Green region represents the experimental results that surpass the standard limit by about 0.7 dB at $N = 12$. Purple circles show the achievable precision for the hybrid sensing scheme with a fit $\log_{10} \delta\theta = -0.91 \log_{10} N + 0.057$, provided all photon numbers can be detected. Error bars are smaller than the markers. The scaling $N^{-0.69}$ (for an ideal experiment) can still beat the standard scaling $N^{-0.5}$ due to the initial MVS. The offset of the hybrid scheme is mainly due to the imperfect photon number detection.

purple circles in Fig. 4c).

Our single-mode quantum metrology architecture achieves a precision near the HL and holds the advantage of hardware efficiency, minimized sensing configuration, and compatibility with quantum error correction that can be employed for further enhancement of the precision [27]. Our scheme can also be directly applied to other physical systems such as trapped ions [28] and nitrogen-vacancy centers [29]. As demonstrated in the hybrid scheme, the precision still beats the SNL with the restricted detecting scheme consisting of only displacement operation and photon counting, which are easy to implement in optics. Additionally if we use microwave-to-optical up- and down-conversion twice, near-HL precisions with the optimal detecting scheme can be achieved. Our scheme thus also adds a powerful new platform to optical quantum metrology, which is quantum resource saving and robust compared to the multiple-path optical interferometer.

This work was supported by the National Key Research Funding No.2017YFA0304303 and the National Natural Science Foundation of China under Grant No.11474177. H.Y. was supported by RGC Hong Kong (Grant No 14207717). C.-L.Z. was supported by National Natural Science Foundation of China (Grant No. 11874342) and Anhui Initiative in Quantum Information Technologies (AHY130000).

* These two authors contributed equally to this work.

[1] V. Giovannetti, S. Lloyd, and L. Maccone, “Advances in quan-

- tum metrology,” *Nat. Photonics* **5**, 222 (2011).
- [2] L. Pezzè, A. Smerzi, M. K. Oberthaler, R. Schmied, and P. Treutlein, “Quantum metrology with nonclassical states of atomic ensembles,” *Rev. Mod. Phys.* **90**, 035005 (2018).
- [3] D. Braun, G. Adesso, F. Benatti, R. Floreanini, U. Marzolino, M. W. Mitchell, and S. Pirandola, “Quantum-enhanced measurements without entanglement,” *Rev. Mod. Phys.* **90**, 35006 (2018).
- [4] K. Jacobs, R. Balu, and J. D. Teufel, “Quantum-enhanced accelerometry with a nonlinear electromechanical circuit,” *Phys. Rev. A* **96**, 023858 (2017).
- [5] N. Ofek, A. Petrenko, R. Heeres, P. Reinhold, Z. Leghtas, B. Vlastakis, Y. Liu, L. Frunzio, S. M. Girvin, L. Jiang, M. Mirrahimi, M. H. Devoret, and R. J. Schoelkopf, “Extending the lifetime of a quantum bit with error correction in superconducting circuits,” *Nature* **536**, 441 (2016).
- [6] L. Hu, Y. Ma, W. Cai, X. Mu, Y. Xu, W. Wang, Y. Wu, H. Wang, Y. Song, C. Zou, S. M. Girvin, L.-M. Duan, and L. Sun, “Demonstration of quantum error correction and universal gate set on a binomial bosonic logical qubit,” *arXiv:1805.09072* (2018).
- [7] S. Chu, “Cold atoms and quantum control,” *Nature* **416**, 206 (2002).
- [8] R. X. Adhikari, “Gravitational radiation detection with laser interferometry,” *Rev. Mod. Phys.* **86**, 121 (2014).
- [9] V. Giovannetti, S. Lloyd, and L. Maccone, “Quantum-enhanced measurements: Beating the standard quantum limit,” *Science* **306**, 1330 (2004).
- [10] R. Schnabel, N. Mavalvala, D. E. McClelland, and P. K. Lam, “Quantum metrology for gravitational wave astronomy,” *Nat. Commun.* **1**, 121 (2010).
- [11] T. Nagata, R. Okamoto, J. L. O’Brien, K. Sasaki, and S. Takeuchi, “Beating the standard quantum limit with four-entangled photons,” *Science* **316**, 726 (2007).
- [12] S. Slussarenko, M. M. Weston, H. M. Chrzanowski, L. K.

- Shalm, V. B. Verma, S. W. Nam, and G. J. Pryde, “Unconditional violation of the shot-noise limit in photonic quantum metrology,” *Nat. Photonics* **11**, 700 (2017).
- [13] M. H. Devoret and R. J. Schoelkopf, “Superconducting circuits for quantum information: An outlook,” *Science* **339**, 1169 (2013).
- [14] K. Duivenvoorden, B. M. Terhal, and D. Weigand, “Single-mode displacement sensor,” *Phys. Rev. A* **95**, 012305 (2017).
- [15] S. L. Braunstein and C. M. Caves, “Statistical distance and the geometry of quantum states,” *Phys. Rev. Lett.* **72**, 3439 (1994).
- [16] A. Facon, E.-K. Dietsche, D. Grosso, S. Haroche, J.-M. Raimond, M. Brune, and S. Gleyzes, “A sensitive electrometer based on a Rydberg atom in a Schrödinger-cat state,” *Nature* **535**, 262 (2016).
- [17] T. Chalopin, C. Bouazza, A. Evrard, V. Makhlov, D. Dreon, J. Dalibard, L. A. Sidorenkov, and S. Nascimbene, “Quantum-enhanced sensing using non-classical spin states of a highly magnetic atom,” *Nat. Commun.* **9**, 4955 (2018).
- [18] E. K. Dietsche, A. Larrouy, S. Haroche, J. M. Raimond, M. Brune, and S. Gleyzes, “High-sensitivity magnetometry with a single atom in a superposition of two circular rydberg states,” *Nat. Phys.* **s41567-018-0405-4**, online (2019).
- [19] H. Paik, D. I. Schuster, L. S. Bishop, G. Kirchmair, G. Catelani, A. P. Sears, B. R. Johnson, M. J. Reagor, L. Frunzio, L. I. Glazman, S. M. Girvin, M. H. Devoret, and R. J. Schoelkopf, “Observation of high coherence in josephson junction qubits measured in a three-dimensional circuit qed architecture,” *Phys. Rev. Lett.* **107**, 240501 (2011).
- [20] R. W. Heeres, B. Vlastakis, E. Holland, S. Krastanov, V. V. Albert, L. Frunzio, L. Jiang, and R. J. Schoelkopf, “Cavity state manipulation using photon-number selective phase gates,” *Phys. Rev. Lett.* **115**, 137002 (2015).
- [21] R. W. Heeres, P. Reinhold, N. Ofek, L. Frunzio, L. Jiang, M. H. Devoret, and R. J. Schoelkopf, “Implementing a universal gate set on a logical qubit encoded in an oscillator,” *Nat. Commun.* **8**, 94 (2017).
- [22] W. Wang, L. Hu, Y. Xu, K. Liu, Y. Ma, S.-B. Zheng, R. Vijay, Y. P. Song, L.-M. Duan, and L. Sun, “Converting quasiclassical states into arbitrary fock state superpositions in a superconducting circuit,” *Phys. Rev. Lett.* **118**, 223604 (2017).
- [23] N. Khaneja, T. Reiss, C. Kehlet, T. Schulte-Herbrüggen, and S. J. Glaser, “Optimal control of coupled spin dynamics: design of NMR pulse sequences by gradient ascent algorithms,” *Journal of Magnetic Resonance* **172**, 296 (2005).
- [24] L. Fan, C.-L. Zou, R. Cheng, X. Guo, X. Han, Z. Gong, S. Wang, and H. X. Tang, “Superconducting cavity electro-optics: A platform for coherent photon conversion between superconducting and photonic circuits,” *Sci. Adv.* **4**, eaar4994 (2018).
- [25] A. P. Higginbotham, P. S. Burns, M. D. Urmey, R. W. Peterson, N. S. Kampel, B. M. Brubaker, G. Smith, K. W. Lehnert, and C. A. Regal, “Harnessing electro-optic correlations in an efficient mechanical converter,” *Nat. Phys.* **14**, 1038 (2018).
- [26] J. C. Matthews, X.-Q. Zhou, H. Cable, P. J. Shadbolt, D. J. Saunders, G. A. Durkin, G. J. Pryde, and J. L. O’Brien, “Towards practical quantum metrology with photon counting,” *npj Quantum Inf.* **2**, 16023 (2016).
- [27] S. Zhou, M. Zhang, J. Preskill, and L. Jiang, “Achieving the Heisenberg limit in quantum metrology using quantum error correction,” *Nat. Commun.* **9**, 78 (2018).
- [28] J. Zhang, M. Um, D. Lv, J.-N. Zhang, L.-M. Duan, and K. Kim, “NOON states of nine quantized vibrations in two radial modes of a trapped ion,” *Phys. Rev. Lett.* **121**, 160502 (2018).
- [29] D. A. Golter, T. Oo, M. Amezcua, I. Lekavicius, K. A. Stewart, and H. Wang, “Coupling a Surface Acoustic Wave to an Electron Spin in Diamond via a Dark State,” *Phys. Rev. X* **6**, 041060 (2016).